



Seismic retrofitting of full-scale RC interior beam-column-slab subassemblies with CFRP wraps



Cailong Ma, Daiyu Wang, Zhenyu Wang*

Key Lab of Structures Dynamic Behavior and Control of the Ministry of Education, Harbin Institute of Technology, Harbin 150090, China
School of Civil Engineering, Harbin Institute of Technology, Harbin 150090, China

ARTICLE INFO

Article history:

Received 15 July 2016
Revised 20 September 2016
Accepted 28 September 2016
Available online 29 September 2016

Keywords:

Fiber reinforced polymer
RC frame
Interior subassembly
Seismic retrofitting
Seismic performance

ABSTRACT

To investigate the effect of carbon fiber-reinforced polymer (CFRP) retrofitting on the failure modes and seismic performance of reinforced concrete (RC) frames, this paper presents the quasi-static test results of four full-scale interior subassemblies with slab and transverse beams. These beam-column-slab subassemblies consisted of one control specimen and three specimens with different CFRP retrofitting schemes. The seismic performance of subassemblies was discussed by comparing failure modes, hysteretic behavior, displacement ductility, stiffness degradation, energy dissipation capacity, shear deformation of joint region and beam vertical deformations. The test results demonstrated that the control specimen finally exhibited column-hinge failure mode due to the existence of slab and transverse beams. After being retrofitted with CFRP, the failure varied to ductile beam-hinge failure mode and the ductility and energy dissipation capacity were enhanced. For the interior beam-column-slab subassemblies, wrapping CFRP wraps at the potential plastic hinge region of columns is a reasonable method for improving the seismic performance and implementing the strong column-weak beam failure mode.

© 2016 Elsevier Ltd. All rights reserved.

1. Introduction

In many earthquakes, the failure of RC joints region and columns end adjacent to it usually led to the partial or total collapse of structures and caused extensive economic and human losses [1–4]. It is noteworthy that some RC frames although designed in accordance with current seismic codes still exhibited the nonductile column failure mode [5–7]. In order to improve seismic performance and the safety of the RC frames, there is an urgent need for seismic retrofitting of the beam-column-slab subassemblies, which are usually chosen as an experimental model and defined as the joint region plus the columns, beams, and slabs adjacent to it [8].

In the past two decades, the externally bonded fiber reinforced polymers (FRP) composites for seismic retrofitting RC structures have been widely used [9,10]. As a result, numerous experimental studies have been conducted on the seismic rehabilitation of RC interior beam-column subassemblies using FRP wraps [11–21]. The experimental models of these studies were mainly beam-column subassemblies without slabs, transverse beams or internal lateral steel reinforcement in the joint region. The purposes of FRP

retrofitting were to prevent or postpone shear failure of joint region and to change the final failure modes into beam hinge mechanism. The efficiency of externally bonded FRP wraps in improving the seismic performance of beam-column subassemblies has been confirmed.

However, it is worth noting that the seismic performance and failure mode of beam-column subassemblies are greatly affected by transverse beams and slab [22–26]. Researches on FRP retrofitted interior beam-columns subassemblies considering the effect of slab and/or transverse beams have so far been limited [27–30]. Wu and Wang [27] experimentally evaluated the efficiency of bonded FRP in improving the shear strength of reduced scale interior beam-column subassemblies. The influence of transverse beams was investigated, however, the contribution of slabs was not considered. The test results indicated that the existence of transverse beam could effectively postpone premature shear failure of the joint core region. Al-Salloum and Almusallam [28] upgraded the shear strength and ductility of substandard interior beam-column subassemblies with slab but no transverse beams by two FRP retrofitting schemes. It was found that the shear failure of joint core region was effectively delayed after being retrofitted with FRP. The negative bending capacity of the beam was also found to be increased due to the existence of slabs. Lu and Yu [29,30] conducted the experiment on the FRP retrofitting of the

* Corresponding author at: School of Civil Engineering, Harbin Institute of Technology, Harbin 150090, China.

E-mail address: zhenyuwang@hit.edu.cn (Z. Wang).

pre-damaged half-scale interior beam-column subassemblies with slab only or both slab and transverse beams. The test results demonstrated that the control subassemblies with slab only exhibited shear failure mode of joint core regions. Although the specimens were designed according to the strong column-weak beam principle [31,32], the specimens with slab and transverse beams failed in column hinge mode. After being retrofitted with FRP, the subassemblies with slab only failed due to the serious damage of the joint core region and beam ends, however, the failure of subassemblies with slab and transverse beams were varied to ductile beam-hinge mode.

From the review of the limited studies above, it is necessary that the specimens are designed with slab and transverse beams to accurately simulate interior beam-column-slab subassemblies of RC frame buildings. Moreover, all of the above studies have addressed FRP retrofitting of beam-column subassemblies with seismic deficiencies or pre-damaged subassemblies. However, many existing RC structures complied with current seismic code might be in need of a retrofitting before earthquakes for some reasons including changes in seismic hazard levels, deteriorations with time and design methods [33]. Against this background, this paper presents the results of an experimental study on the seismic performance of 4 full-scale interior RC beam-column-slab subassemblies retrofitted with carbon fiber reinforced polymer (CFRP) before earthquakes. The subassemblies were designed according to strong column-weak beam principle of the current seismic code [31,32]. The test specimens consisted of a control beam-column-slab subassembly, one specimen wrapped by FRP at column end and two specimens retrofitted with FRP at column end, beams end and slabs. The main objectives of this study were to investigate and evaluate the influence of slab and transverse beams and the different FRP retrofitting schemes on the failure mode and seismic performance of interior RC subassemblies. Finally, the effective and reasonable retrofitting scheme for interior RC subassemblies was recommended based on the experimental results.

2. Experimental program

2.1. Test specimens and material properties

To simulate interior beam-column-slab subassemblies of typical multi-storey RC frame buildings, 4 full-scale specimens were designed and fabricated according to current national seismic design code of China (GB50011-2010). One specimen, namely, the control specimen (i.e. specimen C), was tested first without retrofitting. The rest three specimens were tested after being retrofitted by CFRP with different schemes. All specimens have the identical geometry and reinforcement details as shown in Fig. 1. The cross section of the columns was $400 \times 400 \text{ mm}^2$. All the columns were reinforced with eight 20 mm deformed bars, which resulted in the longitudinal reinforcement ratio of 1.57%. The cross section of the longitudinal beams was $250 \times 600 \text{ mm}^2$. The longitudinal beams were reinforced with two 25 mm and 20 mm deformed bars in the top and bottom of the section, respectively, and four 16 mm bars as torsional reinforcement in the middle of the section. The transverse beams had the section of $250 \times 500 \text{ mm}^2$ and longitudinal reinforced with two 16 mm deformed bars in the top, middle and bottom of the section, respectively. The shear reinforcements in columns and beams were both provided using plain stirrups with 8 mm diameter at 100 mm spacing and 10 mm at 200 mm spacing, respectively. The thickness and width of the slab were 120 mm and 1450 mm, respectively. The slab was reinforced by 10 mm plain bars with 200 mm center to center spacing. The concrete cover was 35 mm, 25 mm, and 15 mm for columns, beams, and slabs, respectively.

The control and retrofitted specimens were produced from two batches of ready-mixed concrete. To obtain the accurate concrete compressive strength, three standard cylinders were cast along with each batch of subassemblies. The average 28-day compressive strength obtained from standard cylinders in accordance with ACI 318-08 [31] was 24.4 MPa and 21.5 MPa for the control and retrofitted specimens, respectively. The mechanical properties of the steel reinforcements were determined from direct tensile tests in accordance with ASTM E8/E8M [34] and given in Table 1. After 28 days curing, unidirectional CFRP with the nominal thickness of 0.167 mm was externally bonded via wet lay-up process for the three retrofitted specimens. The material properties of the CFRP were obtained by testing six flat coupons of 25 mm width and 200 mm length in accordance with ASTM D3039 [35]. The measured average tensile strength and elastic modulus were 4340 MPa and 240 GPa, respectively.

2.2. CFRP retrofitting schemes

To find the efficient and reasonable retrofitting scheme for interior RC subassemblies, three different retrofitting schemes were investigated and evaluated in this study. Although the design of specimens satisfied with the strong column-weak beam principle, the test of the control specimen still exhibited unexpected column-hinge failure mode (more detailed discussions are provided in the next section). According to the observations and main requirements of the national retrofitting design code for concrete structures in China [36,37], three different retrofitting schemes were designed and applied. Before bonding CFRP, the concrete surface was slightly ground and sharp corners of columns and beams were rounded off to a radius of 25 mm at the retrofitting areas.

Fig. 2 shows the retrofitting schemes of all specimens. The first retrofitted specimen, namely SC, was retrofitted by laterally wrapping 3 layers of CFRP only at the potential plastic hinge regions of upper and lower columns with a height of 500 mm and 250 mm, respectively. The second retrofitted specimen, namely SCBU, was retrofitted in the following way: (1) four one-layer L-shaped CFRP strips [sheets 1 and 2 in Fig. 2] with 250 mm width were bonded at plastic hinge regions of columns and beams along the direction of longitudinal reinforcement, which could improve the flexural strength of beam and column; (2) three layers of CFRP sheets with a height of 250 mm and 500 mm [sheets 3 and 4] were wrapped laterally at the potential plastic hinge regions of upper and lower columns; (3) one-layer U-shaped CFRP strips [sheets 5] were applied to each beam end to prevent premature debonding of the L-shaped longitudinal CFRP sheets and to enhance the shear capacity; the lateral CFRP strips [sheets 6] were used to prevent the U-shaped CFRP strips debonding; (4) the U-shaped CFRP strips [sheets 7] were used at the end of transverse beams; four one-layer CFRP strips with 200 mm width [sheets 8] were attached on the surface of slab covered 1400 mm in the longitudinal direction; these straight strips were fixed by six 100 mm width strips [sheets 9] at an interval of 100 mm. The detailed retrofitting scheme of specimen SCBU is shown in Fig. 2(e). For the third retrofitted specimens, namely SCBW, all the retrofitting processes were the same as the specimen SCBU, except the U-shaped strips at the longitudinal beams were replaced by one-layer laterally wrapped CFRP [sheets 10]. To achieve this goal, the slab of the retrofitted area was not cast until the longitudinal beams were wrapped by CFRP sheets. After the beams were retrofitted, the missed slab was cast and cured and then retrofitted with the same scheme as specimen SCBU. The retrofitting process of specimen SCBW are shown in Fig. 3.

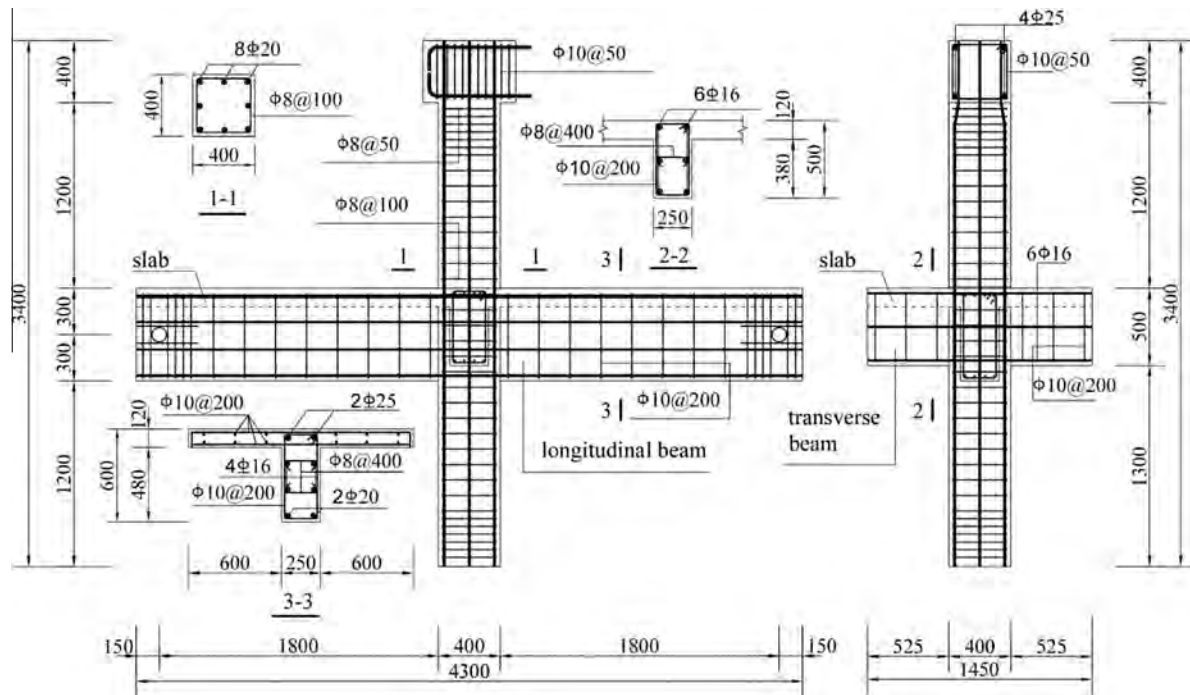


Fig. 1. Dimensions and reinforcement details of specimens.

Table 1
Material properties of steel reinforcements.

| Diameter (mm) | Yield strength (MPa) | Ultimate strength (MPa) | Elastic modulus (GPa) |
|---------------|----------------------|-------------------------|-----------------------|
| 25 | 386 | 521 | 219 |
| 20 | 397 | 567 | 222 |
| 16 | 393 | 593 | 208 |
| 10 | 445 | 688 | 233 |
| 8 | 537 | 717 | 221 |

2.3. Experimental setup and instruments

All the specimens were subjected to constant axial load and reversed lateral load at the top end of the upper column. To simulate actual boundary conditions, the bottom end of the upper column was fixed by a hinge and the longitudinal beams ends were supported by two rollers, which allowed free horizontal movement. The loading schematic diagram of the test is given in Fig. 4. In this study, the axial load was approximately equal to $0.45f_c A_g$, where f_c is the compressive strength of concrete and A_g is the gross cross-sectional area. A designed and built loading apparatus was utilized in order to guarantee the constant axial load and moved with the upper part of the column during testing, as shown in Fig. 5(a). Therefore, the second-order effects (i.e. P-delta effect) could be incorporated and simulated during testing. The reversed lateral load was applied by an electro-hydraulic actuator under displacement control mode. Two different lateral loading schemes were applied considering the different deformation capacity of control and retrofitted specimens, as shown in Fig. 6. The displacement increment was set to be multiples of the numerical yield displacement (Δ_y) of upper RC column. Based on the finite element analysis using the Open System for Earthquake engineering Simulation (OpenSees) software, the value of Δ_y corresponding to the tensile yield of the longitudinal steel bars was found to be 8 mm. For control specimen, the lateral displacement was applied with the increment of $0.5\Delta_y$ and reversed once until reached yield Δ_y , after that each displacement level was reversed twice with the

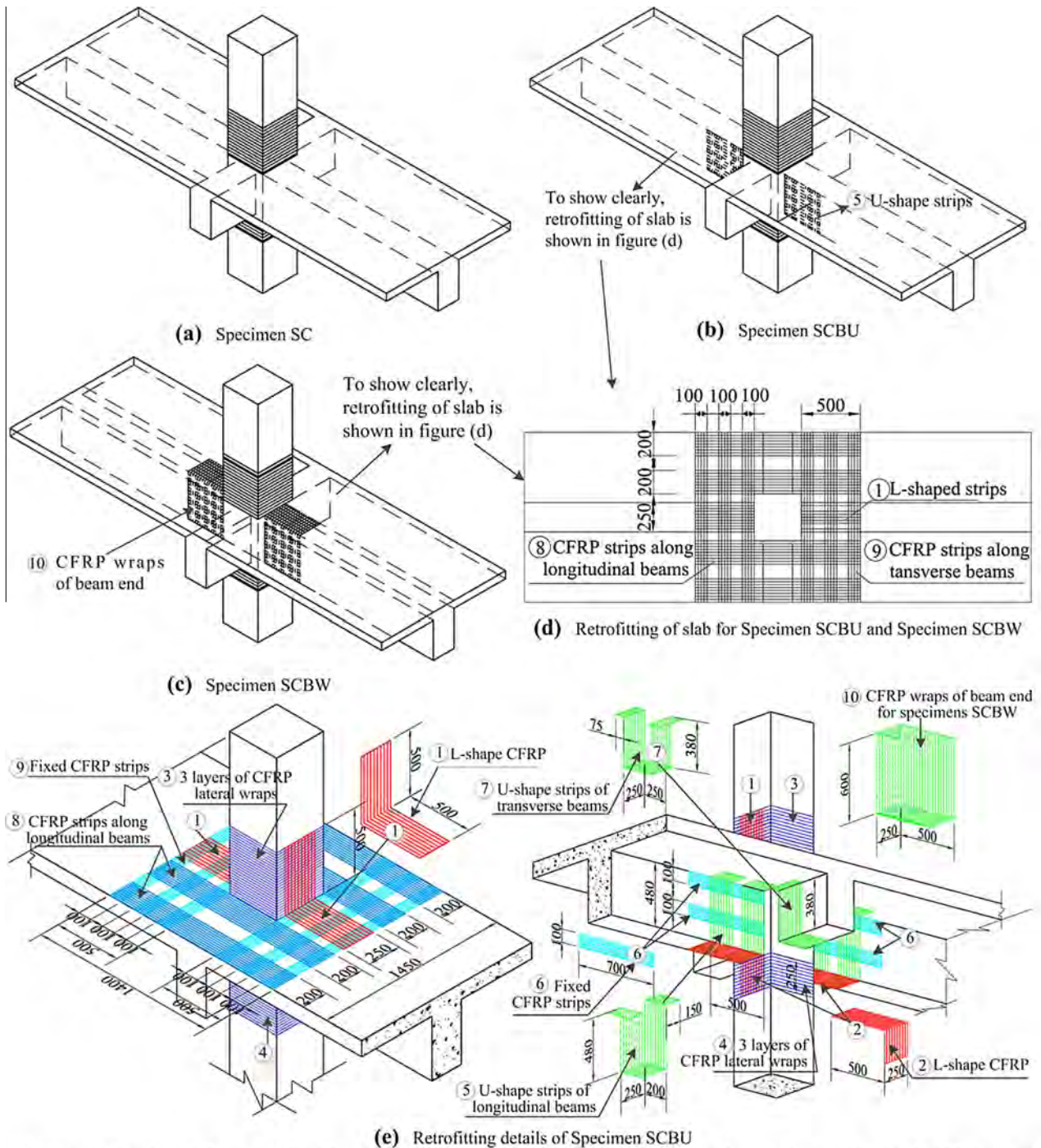
increment of Δ_y . For retrofitted specimens, the first two once reversed cycles were applied with the increment of Δ_y , while the each following displacement level was reversed twice with the increment of $2\Delta_y$. The tests were finally halted if the lateral load dropped to approximately 80% of the peak load.

The load-displacement response was carefully monitored during the tests. The details of the instrumentations layout are illustrated in Fig. 5(b). The lateral displacements of specimens along the height direction were measured by six linear variable displacement transducers (LVDTs) (i.e. C1-C6). Due to the existence of transverse beams and slab, the shear deformation of the joint region was difficult to measure directly. Therefore, a measuring apparatus was designed and installed around the joint region. The shear deformation of the joint region then can be obtained by the measure results of the four LVDTs (i.e. S1-S4). The vertical deformations of the right longitudinal beams were also monitored by the five vertical arranged LVDTs (i.e. B1-B5).

3. Test results and discussions

3.1. Failure of control specimen

The failure modes of the control specimen C are shown in Fig. 7 and a brief summary of the test observations were illustrated as follows. With applying the lateral load, the flexural cracks initially occurred at the plastic hinge regions of longitudinal beams. Then the existing flexural cracks kept developing with increasing width and length and new diagonal shear cracks appeared at the beam ends. In addition, horizontal flexural cracks occurred at plastic hinge regions of upper column end and the surface of the slab. The relative wide splitting at beam-column interfaces was observed at the drift ratio of 1.75%. Bottom longitudinal steel bars of the longitudinal beams were also found to be yielded and slipped at this displacement level. As the lateral drift ratio increased to 2.0%, spalling of concrete cover at the plastic hinge region of the upper column was noticed. The concrete spalling area extended with the increase of lateral displacement. Finally, the



Notes: 1) Specimen SC was retrofitted by wrapping 3 layers of CFRP at the end of upper and lower columns with a height of 500 mm and 250 mm [sheets ③ and ④]; 2) Specimen SCBW has only difference with specimen SCBU that sheets ⑩ instead of sheets ⑤ and ⑥.

Fig. 2. CFRP retrofitting schemes.

plastic hinge was formed at the upper column end. The cover concrete was severely spalled and crushed leading to the exposure of internal hoops and longitudinal steel reinforcements. It was found that the internal hoops have been bent out and the longitudinal bars have been buckled.

It should be noted that the column-to-beam flexural strength ratio ($\Sigma M_{nc}/\Sigma M_{nb}$) of the specimens considering the contribution of slab reinforcement within an effective slab width to the flexural strength of beam end according to ACI 318-08 was 1.94. It means that the design of the specimens conformed with the strong

column-weak beam principle. The experimental phenomena also indicated that the beam end firstly yielded and the final plastic deformation of the specimen C satisfied the limit of the ultimate inter-story drift ratio (i.e. 2%) of RC frames specified by current code of China (i.e. GB 50011-2010). However, the final failure of the control specimen still displayed a “strong beam-weak column” mechanism (i.e. column hinge mode). The main reasons for this phenomenon are analyzed as follows. 1) The steel reinforcements of slabs increased the negative flexural strength capacity of beams and also can bear compressive stress when the beams subjected to



Fig. 3. Pictures showing retrofitted process of specimen SCBW.

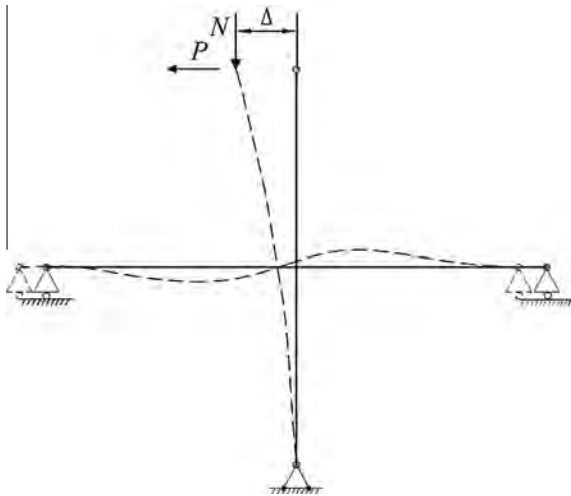


Fig. 4. The schematic plot of loading.

positive bending moment. However, the contribution of steel reinforcement to the compressive stress capacity was not considered in design according to the current code (i.e. GB 50011-2010 or ACI 318-08). This was also the reason that the bottom longitudinal steel reinforcement was yield but the concrete at the top compressive area of the beams was not crushed in the test. 2) Due to the wide splitting of beam-column interfaces, the torsional reinforcements (four 16 mm) of longitudinal beam started to resist moment load together with the longitudinal reinforcements. 3) The presence of transverse beams enhanced the shear resistance capacity

of the joint core area. Moreover, as the support ends of the slabs, the transverse beams effectively restricted the deformation of the slab and further improved the flexural stiffness and capacity of the longitudinal beams.

3.2. Failure of retrofitted specimens

After being retrofitted with CFRP, the failure modes of retrofitted specimens were changed from the unexpected column-hinge mechanism to the expected beam-hinge mechanism. Flexural cracks firstly appeared at the longitudinal beams. The beam-column interface splitting and bottom longitudinal bars yielding and slipping were also observed. With drift ratios increasing, the longitudinal beams were seriously damaged and cover concrete at the corner of joint region partly spalled off. Finally, the ends of longitudinal beams severely damaged and the plastic hinge was developed. Following removal of the CFRP wraps around column ends after the tests, it was evident that the retrofitted part of the column basically remained intact. For specimen SC, the damage was concentrated on the uncovered longitudinal beam ends and joint core region in the form of concrete cover cracking and spalling, especially at the corner areas, as shown in Fig. 8(b) and (c). For specimens SCBU and SCBW, severe concrete spalling occurred at the corners of uncovered joint core region leading to the total exposure of corner longitudinal steel reinforcements of columns, as shown in Figs. 9(b) and 10(b). Serious debonding of the CFRP sheets on the slab was also observed. The bond between CFRP and concrete of slab was almost destroyed at the end of the tests. Specimens SC and SCBU exhibited similar beam-hinge mechanism failure modes. Specimen SCBW failed due to the severe damage of beam end near the support and the beam-column interface.

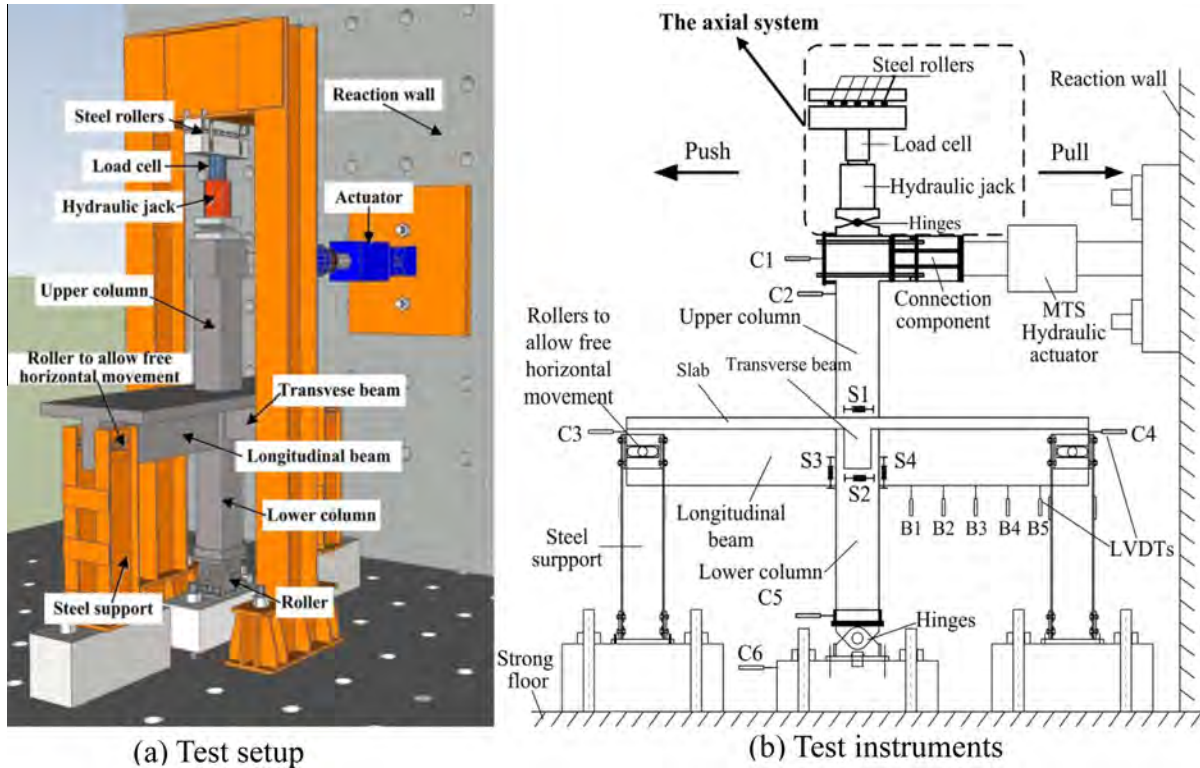


Fig. 5. Test setup and instruments for specimens.

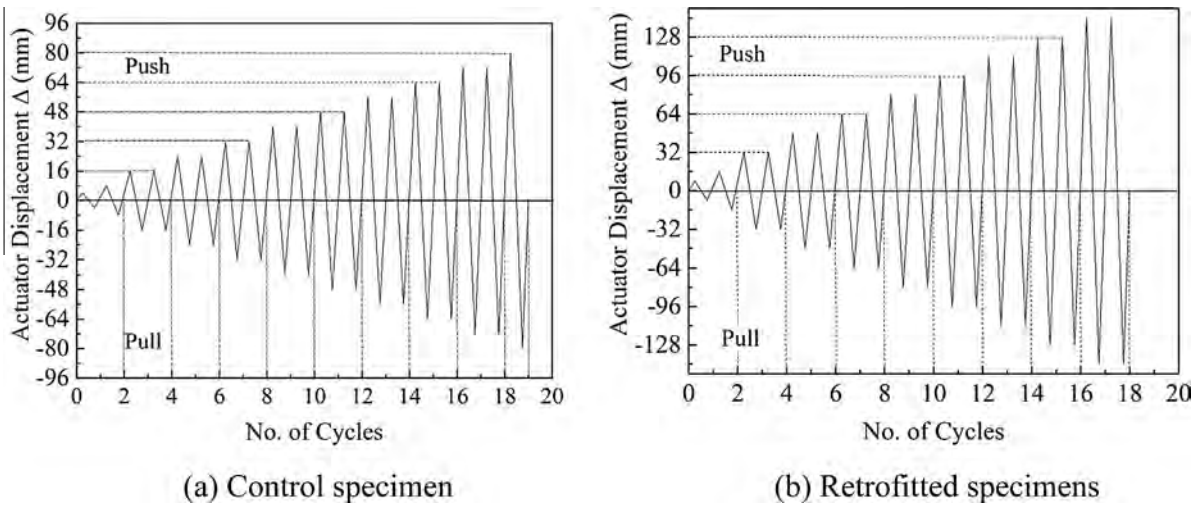


Fig. 6. Cyclic loading schemes.

3.3. Load-displacement hysteretic response

The test lateral load-displacement hysteretic curves of each specimen are shown in Fig. 11. In order to exclude the effect of variation in concrete strength, the lateral load (P) of control specimen C was normalized by multiplying the standard concrete strength ratio of retrofitted specimens to control specimen (is equal to $21.5/24.4 = 0.88$). It can be seen from Fig. 11 that the lateral load-displacement hysteretic behavior of specimen was obviously improved after being retrofitted with CFRP. The lateral resistance capacity was slightly improved, but the deformation and energy dissipation capacity were obviously enhanced. The specimen SC only retrofitted at the column ends exhibited superior hysteretic behavior than the other two retrofitted specimens. Fur-

thermore, pinching and slipping effects can be found in the hysteretic curve for all the specimens, especially at the last stage of the tests. The pinching and slipping effect of retrofitted specimens were also found more obvious than that of the control specimen. This may be mainly attributed to bond-slipping of longitudinal steel bars of beams and the shear deformation of the joint core region. As discussed above, the beam-column interface was found splitting and the bottom longitudinal reinforcement bars of beams yielded and slipped. And also the interface splitting and longitudinal bars bond-slip behavior of retrofitted specimens was larger than that of control specimen. The shear deformation of joint core region was also developed more sufficiently after being retrofitted (more detailed information is presented in the latter section).



Fig. 7. Failure modes of specimen C.



Fig. 8. Failure modes of specimen SC.



Fig. 9. Failure modes of specimen SCBU.



Fig. 10. Failure modes of specimen SCBW.

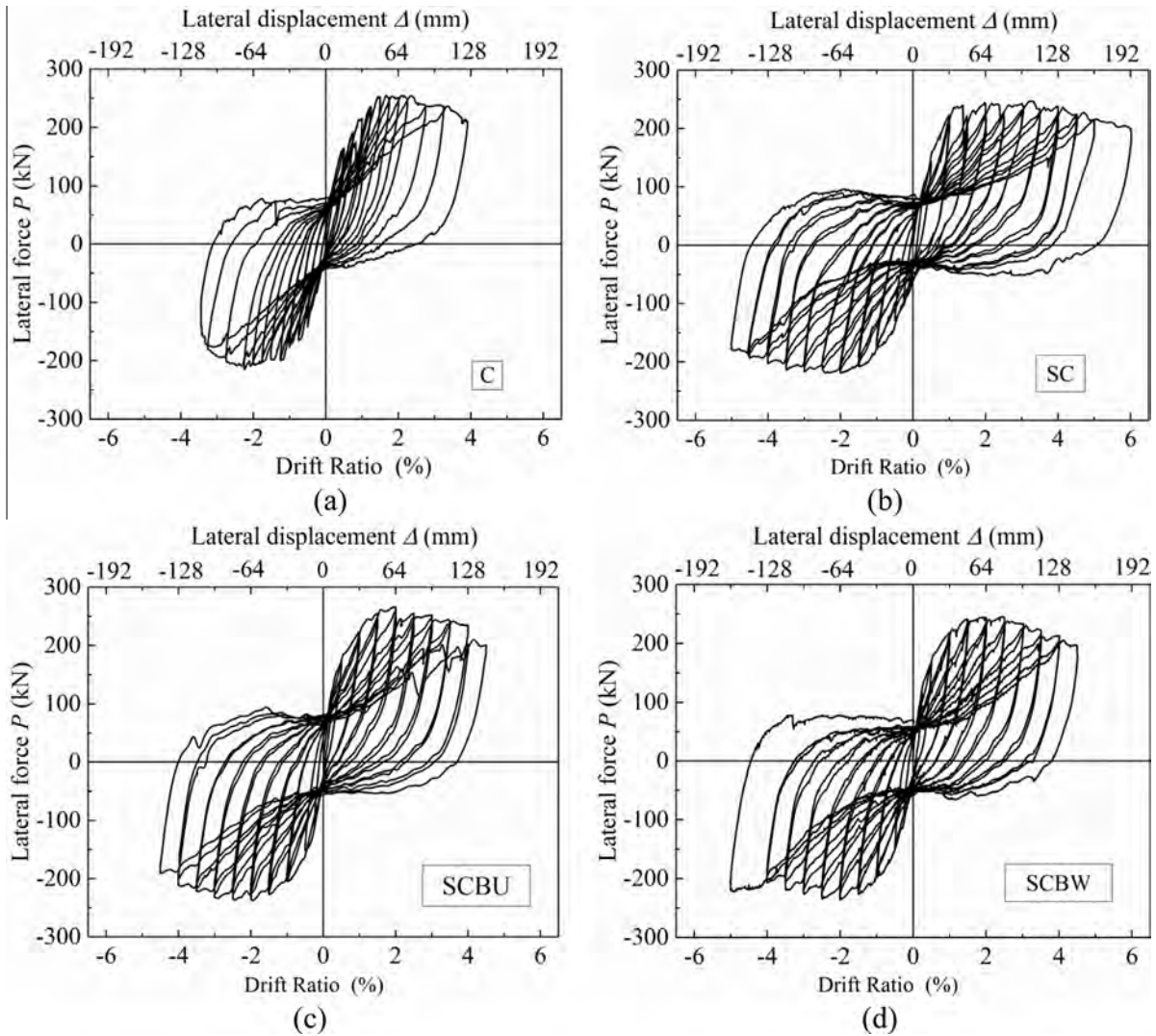


Fig. 11. Load-displacement hysteretic responses.

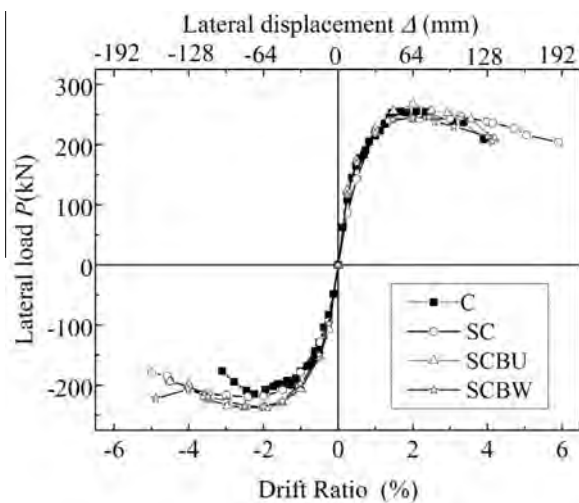


Fig. 12. Load-displacement envelope curves.

3.4. Load-displacement envelopes

Fig. 12 shows the load-displacement envelope curves of the tested specimens, which were obtained from load-displacement hysteretic curves. The main seismic performance indexes of all specimens are summarized in Table 2, and the values of all parameters are the average value in push and pull direction due to the asymmetry of test envelope curves. The yield point is defined by using the energy equivalent method [38]. The ultimate displacement (Δ_u) and corresponding drift ratio (δ_u) were obtained from the point where the lateral load reduced to 85% of the peak load (P_c). The ductility ratio (μ) is equal to the ratio of ultimate displacement (Δ_u) to the yield displacement (Δ_y).

As illustrated in Table 2, the CFRP retrofitting schemes have little influence on the yield displacement (Δ_y) and the yield load (P_y). The peak displacements (Δ_c) of retrofitted specimens were larger than that of specimen C, and the peak drift ratios were about 2% for all the specimens. However, compared with the control specimen C, the ultimate displacements (Δ_u) of specimen SC, SCBU, and SCBW increased by 49%, 16%, and 19.8%, respectively, and the ultimate drift ratios met the requirement of the ultimate inter-story drift ratio (i.e. 2%) of RC frame structures specified by the national seismic design code of China (i.e. GB50011-2010). The ductility ratio (μ) of specimen SC, SCBU, and SCBW were

Table 2
Main seismic performance indexes of specimens.

| Specimen | Δ_y (mm) | P_y (kN) | Δ_c (mm) | P_c (kN) | Δ_u (mm) | Δ_y/H (%) | μ | δ (%) | $\Delta\mu$ | $\Delta\delta$ |
|----------|-----------------|------------|-----------------|------------|-----------------|------------------|-------|--------------|-------------|----------------|
| C | 32.1 | 197.3 | 62.6 | 235 | 107.9 | 1.00 | 3.37 | 3.37 | – | – |
| SC | 33.9 | 203.7 | 73.5 | 232.8 | 160.9 | 1.06 | 4.74 | 5.03 | 41.03 | 49.11 |
| SCBU | 30.9 | 211.6 | 63.1 | 252.3 | 125.3 | 0.97 | 4.05 | 3.91 | 20.46 | 16.12 |
| SCBW | 30.3 | 202.3 | 71.1 | 240.8 | 129.3 | 0.95 | 4.27 | 4.04 | 27.03 | 19.85 |

Note: P_y = normalized yield load; P_c = normalized peak load; Δ_y = yield displacement; Δ_c = peak displacement; Δ_u = ultimate displacement; μ = displacement ductility ratio; δ = ultimate drift ratio; $\Delta\mu$ = increment of displacement ductility ratio; $\Delta\delta$ = increment of ultimate drift ratio.

increased by 41%, 20% and 27% compared with that of control specimen, respectively. The plastic deformation capacity of the specimens was significantly improved after being retrofitted by CFRP, especially for specimen SC. It is evident that retrofitting of the plastic hinge regions of columns is the most effective technical in improving the seismic performance of interior RC beam-column-slab subassemblies among the three retrofitting schemes.

3.5. Stiffness degradation

The stiffness degradation is usually attributed to concrete non-linear deformations, concrete cracking, yielding of longitudinal bars, steel reinforcement bonding-slippage. The degradation of effective stiffness (K_{eff}), which is defined as the secant stiffness at the unloading point of each displacement level, is shown in Fig. 13. It is indicated that specimen SCBW and SCBU exhibited larger effective stiffness than that of specimen C and SC in the initial stage of lateral loading. Moreover, the control specimen C and retrofitted specimen SC had approximately the same effective stiffness and its degradation. The main reason is that the CFRP sheets [sheets 5 and 6] effectively delayed the flexural cracks of longitudinal beams for specimen SCBU and specimen SCBW, and then delayed the stiffness degradation. As the drift ratio increased larger than 2.5%, the effective stiffness degradation behavior was approximately the same for all the specimens. This is due to the longitudinal reinforcements had slipped before the drift ratio of 2.5% and no new cracks generated after the drift ratio of 2.5%. In general, the results indicate that the FRP retrofitting has little influence on the effective stiffness of specimens.

3.6. Energy dissipation

The energy dissipation capacity is one of the other important seismic performance indicators for structure. In this study, cumulative energy dissipation was computed by summing the

enclosed area within load-displacement loop of the first cycle at each drift ratio. Fig. 14 shows the cumulative energy dissipation versus drift ratio curves for all tested specimens. After the drift ratio increased up to 1%, the single-loop energy dissipation of retrofitted specimens was apparently larger than that of the control specimen C. The cumulative energy dissipation of retrofitted specimens was greatly larger than that of the control specimen C. The single-loop energy dissipation of specimens SCBU and SCBW was larger than that of specimen SC at a certain drift ratio over 3%, but the cumulative energy dissipation was less than that of specimen SC. This indicates that the energy dissipation capacities of retrofitted specimens were improved and specimen SC has the largest energy dissipation capacity among all the retrofitted specimens.

3.7. Shear force of joint region

The shear force across the mid-depth of the joint core region (V_{jh}) for each specimen was estimated according to the proposed methods adopted by ACI 352R-02 [1], as illustrated in Fig. 15. The expression of V_{jh} is given as follows:

$$V_{jh} = T_{b1} + T_{s1} + T_{s2} + C_{b2} - V_{col1} \tag{1}$$

$$T_b + T_{s1} + T_{s2} = f_{yb}A_{b1} + f_{ys}A_{s1} + f_{ys}A_{s2} \tag{2}$$

$$C_{b2} = T_{b2} = f_{yb}A_{b2} \tag{3}$$

where V_{col1} and V_{col2} = shear force in the column, calculated using the conditions of equilibrium; T_{b1} and T_{b2} = tensile force in the beam; C_{b1} and C_{b2} = compressive force in the beam; T_{s1} and T_{s2} = tensile force in the slab; f_{yb} = yield stress of reinforcements in the beam; f_{ys} = yield stress of reinforcements in the slab; A_{b1} and A_{b2} = area of longitudinal reinforcements in the beam; A_{s1} and A_{s2} = area

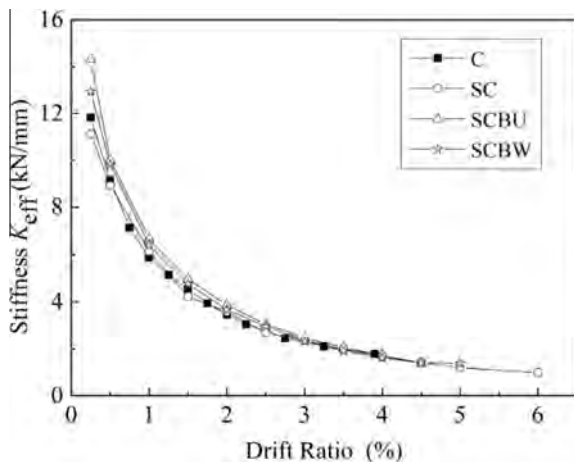


Fig. 13. Stiffness degradation of tested specimens.

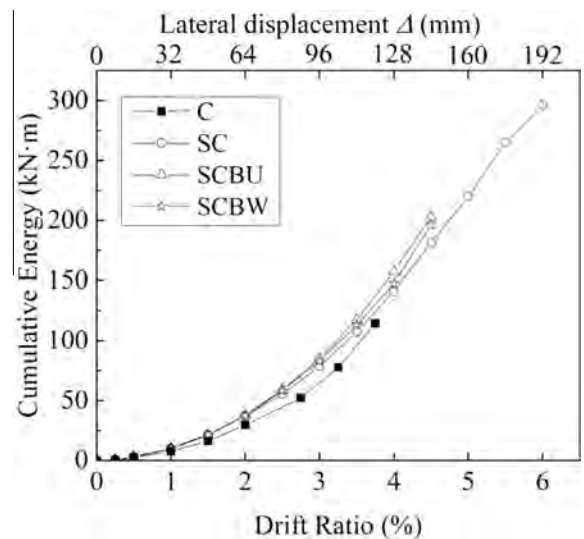


Fig. 14. Cumulative energy dissipation.

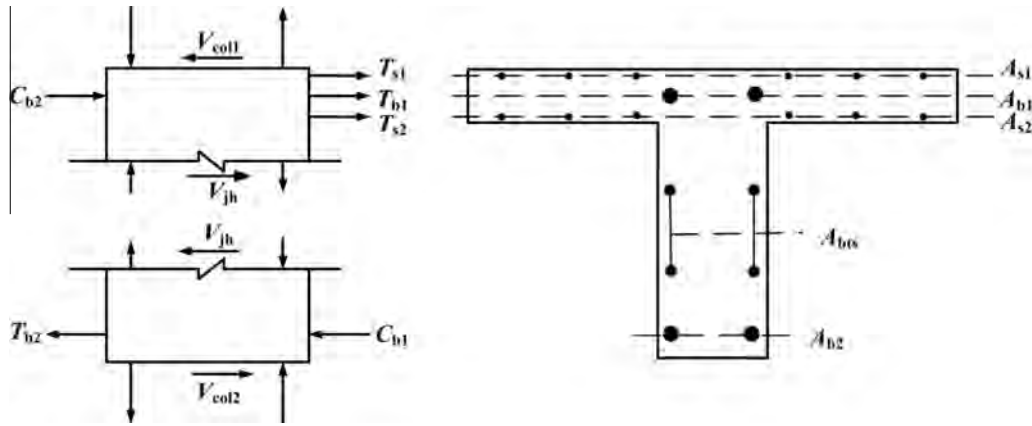


Fig. 15. Evaluation of horizontal joint shear force.

of reinforcements in the slab; A_{bt5} = area of torsional reinforcements in the beam; The calculated shear force of V_{jh} should be less than or equal to the nominal shear force of the joint core region, as expressed in Eq. (4), which specified by ACI 352R-02 and ACI 318-08.

$$\phi V_n \geq V_{jh} \quad (4)$$

where $\phi = 0.85$, strength reduction factor; V_n = the nominal shear force of the joint region, is calculated as follows:

$$V_n = 0.083\gamma\sqrt{f'_c}b_jh_c \quad (5)$$

where $\gamma = 20$, factor based on the type of joint, which is provided in ACI 318-08; f'_c = compressive strength of concrete; b_j = effective width of the joint region; h_c = depth of column in the direction of the shear.

The calculated shear force in the joint core area of each specimen is presented in Table 3. It is evident that the nominal shear forces (V_n) were larger than the horizontal shear force (V_{jh}) for all the specimens. In other words, it means that the joint shear failure would not appear for all the specimens, even though the joint core regions of retrofitted specimens were not retrofitted. This result is consistent with the previous discussed experimental observations that the retrofitted specimens generally exhibited beam hinge failure mechanism and no shear failure of joint core area was observed. It is then can be concluded that the joint region does not need to be retrofitted if the interior beam-column-slab sub-assembly satisfied with the current seismic code (i.e. ACI 318-08, GB 50011-2010).

3.8. Shear deformation of joint region

The average joint shear deformation γ_j can be estimated based on the deformed shape of the joint region, as illustrated in Fig. 16. The definition of γ_j is therefore defined as follows:

$$\gamma_j = \gamma_1 + \gamma_2 = \frac{\delta}{h_j} + \frac{\delta'}{b_j} \quad (6)$$

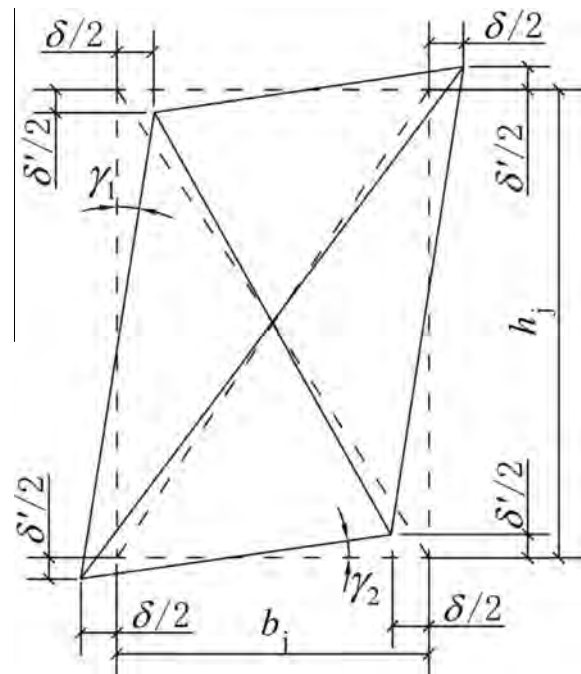


Fig. 16. Estimation of average joint shear deformation.

where δ and δ' = relative deformation in the horizontal direction and vertical direction, respectively; h_j and b_j = the height and width of the joint region, respectively.

To obtain average joint shear deformation, the four LVDTs (see Fig. 5(b)) must monitor and record the deformation responses simultaneously. However, due to one LVDT was damaged during the test, the average joint shear deformation of specimen SC was failed to measure. Fig. 17 shows the average shear deformations of control specimen C and retrofitted specimen of SCBU and SCBW.

Table 3
Joint region shear forces for tested specimens.

| Shear forces | Symbol (kN) | Specimen | | | |
|--|----------------|----------|-----|------|------|
| | | C | SC | SCBU | SCBW |
| Column shear force | V_{col1} | 235 | 232 | 252 | 240 |
| Horizontal shear force of joint region [Eq. (1)] | V_{jh} | 812 | 815 | 795 | 807 |
| Nominal joint shear force [Eq. (5)] | ϕV_n | 905 | 850 | 850 | 850 |

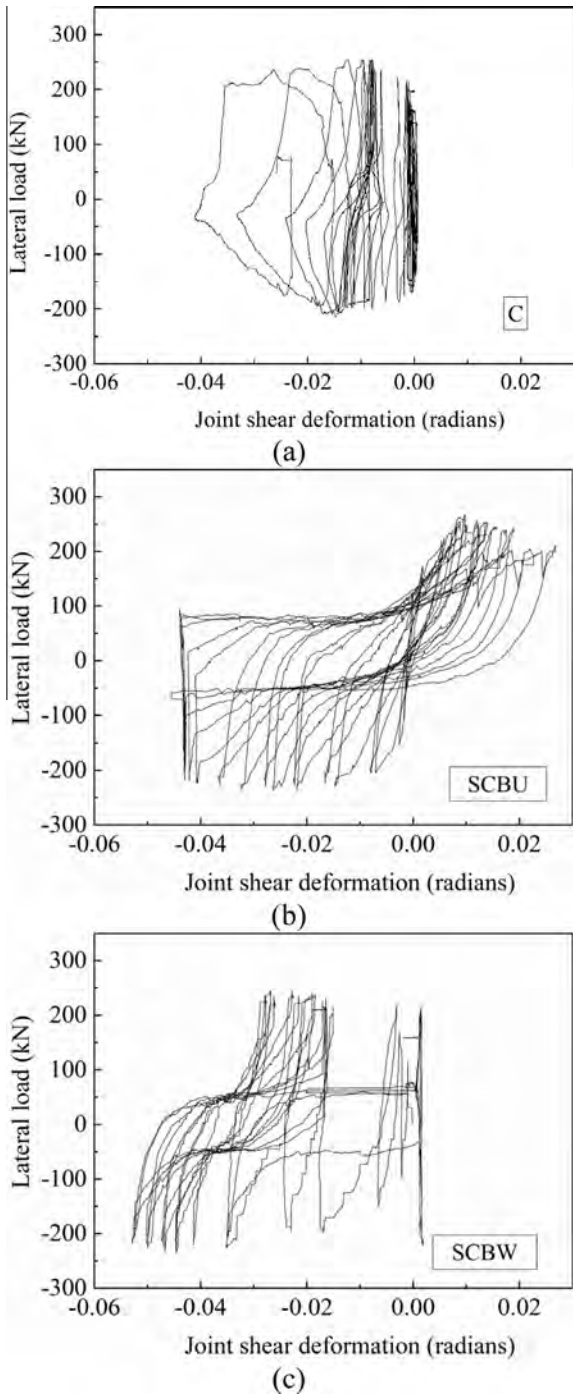


Fig. 17. Average joint shear deformation.

For the specimen C, the measured shear deformation was larger than the actual value at the last drift ratio, because the upper column end of specimen C was severely damaged and largely deformed. At the initial stage of loading, all specimens exhibited similar shear deformation responses with relatively smaller values. As the displacement reached to the elastic-plastic stage, the shear deformations of the retrofitted specimens were larger in comparison with that of the control specimen C, especially in the final stage. It indicated that the external bonded CFRP could effectively prevent the column hinge failure mode, but it will also increase the shear deformation of joint core regions. The reasons are summarized as follows: 1) the stiffness degradation of retrofitted columns

and beams were postponed. In this case, the stiffness ratio of joint core regions to the retrofitted columns and beams was reduced. It means that the joint core region becomes relatively weaker; 2) the developing of beam hinge in the last loading stage reduced the confinement to the joint core regions.

3.9. Beam vertical deformation

The vertical deformations of longitudinal beams were mainly the flexural deformations. Fig. 18 shows the vertical deformation responses of longitudinal beams of specimen C, SC, and SCBU at elastic, yield, peak and ultimate point. For the specimen C, the

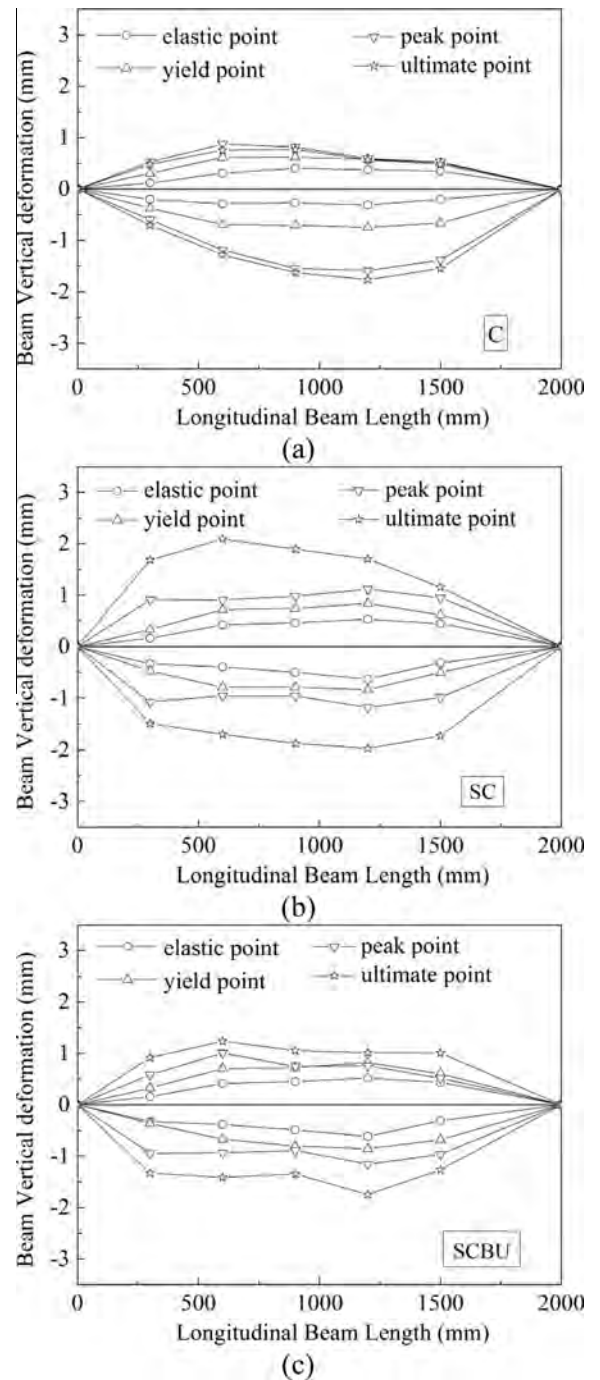


Fig. 18. Beam vertical deformations.

beam vertical deformations at peak point were approximately equal to that at ultimate point and the deformation in negative direction was larger than that in positive direction. The main reasons for this were: 1) the failure of the control specimen concentrated on the upper column end after the drift ratio of 2.0% and the beam end hinge failed to form; 2) the existence of slab increased the negative bending stiffness of longitudinal beam; 3) the existence of transverse beams as the supports of slabs effectively restricted the deformation of slabs, then the composite effect of transverse beams and slabs further increased the bending stiffness of longitudinal beams.

For retrofitted specimens, the beam vertical deformations at the ultimate point were larger than that at the peak point, especially for specimen SC. In addition, the deformations in negative and positive direction were approximately the same at the same drift ratio level. The comparison of vertical deformation of longitudinal beams between control and retrofitted specimens indicated that the deformation of retrofitted specimens was larger than that of control specimen. This attributed to the damage of retrofitted specimens mainly concentrated on the plastic hinge regions of longitudinal beams and slabs, which reduced the flexural stiffness of the beams and further increased the deformation. It is also found that the beam vertical deformation of retrofitted specimen SCBU was smaller than that of the retrofitted specimen SC due to the retrofitting of the longitudinal beams and slab, especially the L-shaped CFRP strips [sheets 1 and 2] at plastic hinge regions of columns and beams along the longitudinal direction.

4. Conclusions

This paper carried out the experimental study on the seismic performance of full-scale RC interior beam-column-slab subassemblies retrofitted with CFRP before earthquakes. The specimens were designed according to current national seismic design code of China (GB50011-2010) to simulate commonly existed interior beam-column-slab subassemblies of typical multi-storey RC frame buildings across China. The main objectives of this study were to investigate and evaluate the influence of slab and transverse beams and the different FRP retrofitting schemes on the failure modes and seismic performance of interior subassemblies. The failure modes, hysteretic behavior, ductility, stiffness degradation, energy dissipation capacity and deformation of the joint core region and longitudinal beams were compared and investigated in detail. The following conclusions can be drawn:

1. The interior beam-column-slab subassemblies designed according to the current Chinese code GB50011-2010 could satisfy the limit of the ultimate drift ratio (i.e. 2%), but the control specimen finally exhibited column-hinge failure mode, which is an unexpected “strong beam-weak column” mechanism. In order to really achieve strong column-weak beam design, it is recommended that the contributions of the slab, transverse beams, and the torsional reinforcements of the longitudinal beam to the flexural strength of longitudinal beam should be sufficiently considered.
2. After being retrofitted with CFRP, the failure of specimens was successfully changed to the expected ductile beam-hinge mechanism. The CFRP retrofitting methods have little effect on the lateral resistance capacity, but obviously improve the energy dissipation and ductility capacity of the interior beam-column-slab subassemblies.
3. For interior beam-column-slab subassemblies that satisfied with the current seismic code, the joint region does not need to be retrofitted due to the existence of transverse beams and enough transverse hoops. Even the column end, the beam end and the slab adjacent to the joint region were retrofitted by CFRP, the core concrete of joint regions still remained intact and no shear failure of joint core region was observed.
4. The comparison of retrofitted specimens with different retrofitting schemes demonstrated that only the potential plastic hinge regions of columns were retrofitted specimen exhibited the best seismic performance. Therefore, to effectively prevent column-hinge mechanism and improve the seismic performance of interior joint subassemblies, lateral wrapping FRP around the potential plastic hinge regions of column ends was the reasonable and recommended method.

Acknowledgments

This study is financially supported by the National Natural Science Foundation of China (Grant Nos. 51478143, 51408153 and 51278150) and the National Key Basic Research Program of China (973 Program, Grant No. 2012CB026200) and China Postdoctoral Science Foundation (Grant Nos. 2014M551252 and 2015T80354).

References

- [1] Durrani AJ, Wight JK. Behavior of interior beam-to-column connections under earthquake-type loading. *J Am Concr Inst* 1985;82(3):343–9.
- [2] Melo J, Varum H, Rossetto T. Cyclic behaviour of interior beam-column joints reinforced with plain bars. *Earthquake Eng Struct Dyn* 2015;44(9):1351–71.
- [3] Somma G, Pieretto A, Rossetto T, Grant DN. RC beam to column connection failure assessment and limit state design. *Mater Struct* 2015;48(4):1215–31.
- [4] Wang G, Dai JG, Teng JG. Shear strength model for RC beam-column joints under seismic loading. *Eng Struct* 2012;40:350–60.
- [5] Arslan MH, Korkmaz HH. What is to be learned from damage and failure of reinforced concrete structures during recent earthquakes in Turkey? *Eng Fail Anal* 2007;14(1):1–22.
- [6] Chung L, Chen Y, Sun C, Lien K, Wu L. Applicability investigation of code-defined procedures on seismic performance assessment of typical school buildings in Taiwan. *Eng Struct* 2012;36:147–59.
- [7] Duan H, Hueste MBD. Seismic performance of a reinforced concrete frame building in China. *Eng Struct* 2012;41:77–89.
- [8] American Concrete Institute (ACI). Recommendations for Design of Beam-Column Connections in Monolithic Reinforce Concrete structures, ACI 352R-02, Farmington Hills, MI, USA; 2002.
- [9] Shrestha R, Smith ST, Samali B. The effectiveness of FRP strips in repairing moderately and severely damaged RC beam-column connections. *Mag Concrete Res* 2011;63(9):629–44.
- [10] Boushelham A. State of research on seismic retrofit of RC beam-column joints with externally bonded FRP. *J Compos Constr* 2010;14(1):49–61.
- [11] Geng ZJ, Chajes MJ, Chou TW, Pan D. The retrofitting of reinforced concrete column-to-beam connections. *Compos Sci Technol* 1998;58(8):1297–305.
- [12] Mosallam AS. Strength and ductility of reinforced concrete moment frame connections strengthened with quasi-isotropic laminates. *Compos Part B-Eng* 2000;31(6–7):481–97.
- [13] Prota A, Nanni A, Manfredi G, et al. Selective upgrade of under-designed reinforced beam-column joints using carbon fiber-reinforced concrete. *ACI Struct J* 2004;101(6):699–707.
- [14] Mukherjee A, Joshi M. FRPC reinforced concrete beam-column joints under cyclic excitation. *Compos Struct* 2005;70(2):185–99.
- [15] Pantelides CP, Okahashi Y, Reaveley LD. Seismic rehabilitation of reinforced concrete frame interior beam-column joints with FRP composites. *J Compos Constr* 2008;12(4):435–45.
- [16] Shiohara H, Kusuhara F, Tajiri S, Fukuyama H. Seismic retrofit of reinforced concrete beam-column joints with CFRP composites. In: ATC & SEI 2009 Conference on Improving the Seismic Performance of Existing Buildings and Other Structures; 2009. p. 1449–59.
- [17] Lee WT, Chiou YJ, Shih MH. Reinforced concrete beam-column joint strengthened with carbon fiber reinforced polymer. *Compos Struct* 2010;92(1):48–60.
- [18] Li B, Chua HYG. Seismic performance of strengthened reinforced concrete beam-column joints using FRP composites. *J Struct Eng* 2009;135(10):1177–90.
- [19] Li B, Kai Q. Seismic behavior of reinforced concrete interior beam-wide column joints repaired using FRP. *J Compos Constr* 2011;15(3):327–38.
- [20] Li B, Kai Q, Xue W. Effects of eccentricity on the seismic rehabilitation performance of nonseismically detailed interior beamwide column joints. *J Compos Constr* 2012;26(5):507–19.
- [21] Esmaeeli E, Barros JAO, Sena-Cruz J, Fasan L, Liprizzi FR, Melo J, Varum H. Retrofitting of interior RC beam-column joints using CFRP strengthened SHCC: cast-in-place solution. *Compos Struct* 2015;122:456–67.

- [22] Ehsani MR, Wight JK. Effect of transverse beams and slab on behavior of reinforced concrete beam-to-column connections. *ACI J Proc* 1985;82(2):188–95.
- [23] Durrani AJ, Wight JK. Earthquake resistance of reinforced concrete interior connections including a floor slab. *ACI Struct J* 1987;84(5):400–6.
- [24] Ammerman OV, French CW. R/C beam-column-slab subassemblages subjected to lateral loads. *J Waterw Port Coastal Ocean Eng* 1989;115(6):1289–308.
- [25] Cheung PC, Paulay T, Park R. New Zealand tests on full-scale reinforced concrete beam-column-slab subassemblages designed for earthquake resistance. 1991;123:1–38.
- [26] French CW, Moehle JP. Effect of floor slab on behavior of slab-beam-column connections. Farmington Hills, ACI design of beam-column joints for seismic resistance. 1991;123:225–258
- [27] Wu B, Wang WJ. An experimental study on the seismic behavior of beam-column joints strengthened with carbon fiber sheets. *China Civil Eng J* 2005;38(4). 60–65,83. (in Chinese).
- [28] Al-Salloum YA, Almusallam TH. Seismic response of interior RC beam-column joints upgraded with FRP sheets. I: Experimental study. *J Compos Constr* 2007;11(6):575–89.
- [29] Yu JT, Lu ZD, Zhang KC. Experimental study on seismic behavior of strengthened RC column-beam joints damaged by simulated earthquake. *China Civil Eng J* 2010;31(12):64–73 (in Chinese).
- [30] Lu ZD, Su L, Yu JT. Experimental study on the seismic behaviour of strengthened concrete column-beam joints by simulated earthquake. *Proc Eng* 2011;14:1871–8.
- [31] American Concrete Institute (ACI). Building code requirements for structural concrete. ACI 318–08, Farmington Hills, MI, USA; 2008.
- [32] Code of China. Code for design of concrete structures, GB 50010–2010. Beijing: Publishing House of Building Industry in China; 2010 (in Chinese).
- [33] Eslami A, Ronagh HR. Experimental investigation of an appropriate anchorage system for flange-bonded carbon fiber-reinforced polymers in retrofitted rc beam-column joints. *J Compos Constr* 2014;18(4):0130564.
- [34] American Society for Test and Materials (ASTM). Standard test methods for tension testing of metallic materials. West Conshohocken, PA, USA: ASTM E8/E8M; 2008.
- [35] American Society for Test and Materials (ASTM). Standard test method for tensile properties of polymer matrix composite materials. West Conshohocken, PA, USA: ASTM D3039/D3039M-08; 2008.
- [36] Code of China. Design code for strengthening concrete structure, GB 50367–2006. Beijing: Publishing House of Building Industry in China; 2006 (in Chinese).
- [37] Code of China. Technical specification for strengthening concrete structures with carbon fiber reinforced polymer laminate, CECS 146:2003. Beijing: The Standardization Institute of Chinese Construction; 2003 (in Chinese).
- [38] Cai ZK, Wang DY, Smith ST, Wang ZY. Experimental investigation on the seismic performance of GFRP-wrapped thin-walled steel tube confined RC columns. *Eng Struct* 2016;110:269–80.